ON AXIS AND OFF AXIS PSF ANALYSIS

PANTER CAMPAIGN – MOS-FM1

EPIC-MCT-TN-001 **Simona Ghizzardi**

October 13, 1999

S. Ghizzardi - Milano Calibration Team - Istituto di Fisica Cosmica - CNR - Milano
e-mail: simona@ifctr.mi.cnr.it

Contents

1 Introduction

In this document, I present a detailed documentation on the calibration of the on-axis and off-axis PSF for MOS–FM1. The analysis is based on available ground calibration measurements from the campaign held in Panter in January 1998. Data are available for 4 different lines: Al–K, Cu–K, Fe–L, Fe–K and for Full Frame (FF) or Partial (200x200) Window (PW) modes. Several RUNS with different exposure times and different count rates have been taken so the behaviours of the PSF related to the pile-up degree can be investigated.

The document is organized according the following main topics

- In Sec. 2 we deal with a general recognition of one single RUN, for a preliminary investigation of the PSF behaviour before carrying out a systematic analysis of all the available data.
- In Sec. 3 we describe the automatic algorithms used for the systematic analysis of both on-axis and off-axis PSF modelization. Results concerning on–axis PSF are reported and discussed. The PSF behaviour at different energies is analyzed.
- In Sec. 4 we reported the results from the systematic analysis for the off-axis PSF (at each off axis angle).
- In Sec. 5, for data at 1.49 keV, we study the behaviour of the PSF at different off-axis angles.

2 Initial recognition: a King profile for the on-axis PSF

Before carrying out a systematic analysis of all the data, we performed a global recognition of one RUN (RUN 01351), which is a measurement at 0.7 keV (Fe–L line). It is a Full Frame, all night long measurement comprising roughly 60000 counts. Almost all the analysis is performed by using IDL software program and it is based on Steve Sembay's procedures for the analysis of MOS calibration data.

In Fig. 1 we plotted the pattern distribution, normalized to the total counts for the events of RUN 01351. It is a first indication of the pile–up degree. The main contribution to data is from monopixels and bipixels pattern configurations, so we can infer that the count rate is quite low and pile–up effects are not significantly involved.

In Fig. 2 we plotted (black curve) the energy spectrum for this RUN. The main peak (700 eV) is the L_α line for Fe but some other peaks are present. The red curve draws the spectrum when only events belonging to a circular region centered in (305, 305) with a radius of 60 pixels are selected. The peak at 520 eV is still completely present and it seems

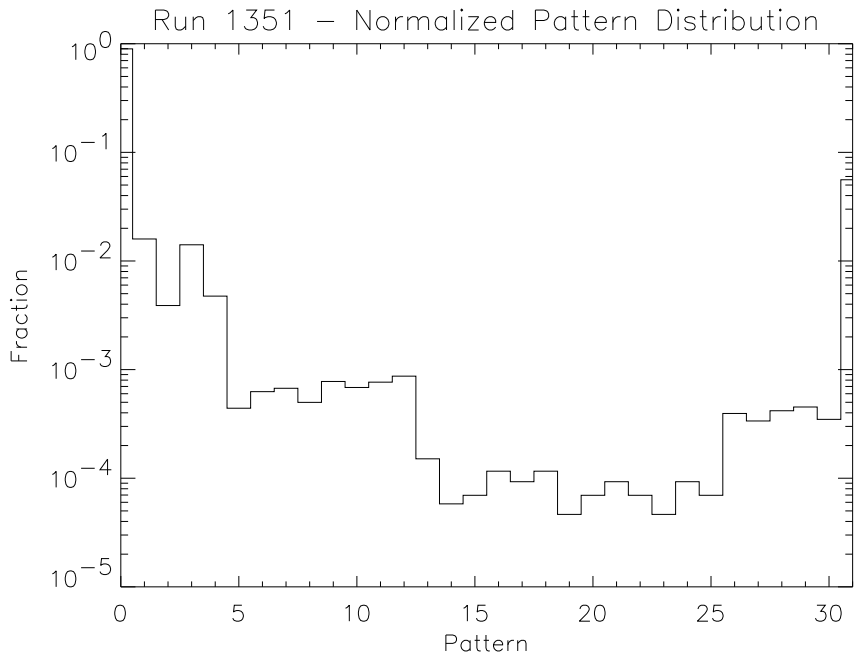

Figure 1: Pattern distribution: the presence of high–labeled patterns is an indication of pile–up.

to be related to the central spot. The peak at 120 eV is still present, but it is smaller. In this peak the ratio between the two spectra is equal to the ratio of the total area of the CCD and the area within the 60 pixels radius. Hence this peak is produced by the background noise. In the range 1-2 keV the bremsstrahlung contribution can be observed. Whenever the statistics in such a range is enough, it can be used to study PSF properties at the corresponding energies. As far as the peak at 210 eV is concerned, the contribution comes completely from three pixels: (125,39); (209, 253); (465, 491) (green, pink, blue curves). So I rejected these three bad pixels as bright pixels, filtering the events.

A confirmation of the absence of pile–up effect comes from the contribution to the energy spectrum (see Fig. 3) coming from each class of pattern configuration (the division is made according to: monopixels, bi-pixels, tri-pixels, 4-5pixels, diagonal configuration, patterns 30-31). As expected, the main contribution comes from monopixels and bipixels. A little contribution for diagonal configuration is present at the double of the main peak-energy, corresponding to piled-up events. Such a contribution is here not very important and also the contribution of higher level patterns is negligible.

Aiming to a characterization of the PSF, our main purpose consists of building its radial profile. In our analysis, only monopixels and bipixels are considered, since other patterns are negligible or related to pile-up effects. Furthermore, an energy range must be selected. In fact, different energy ranges are expected to provide different radial profiles.

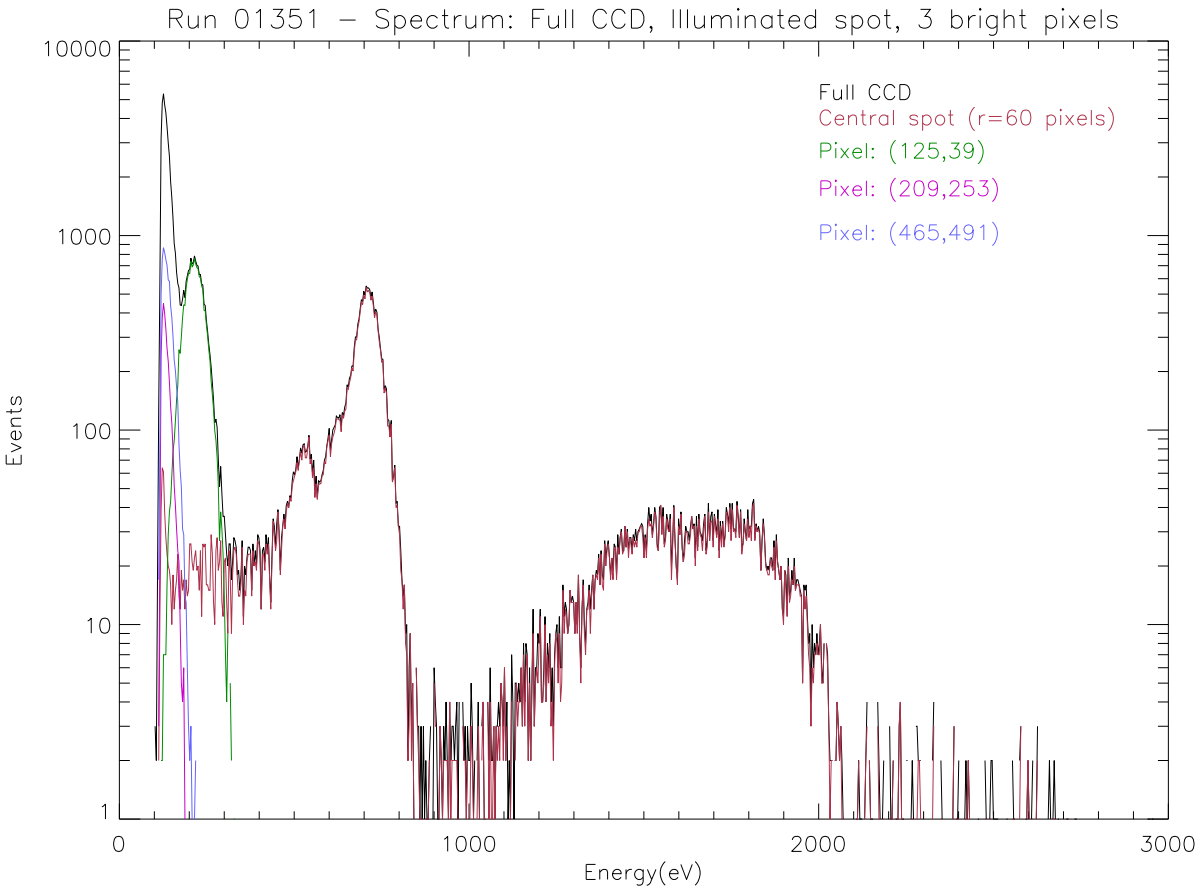

Figure 2: Energy spectrum. The main peak (0.7 keV) corresponds to the L_α line for Fe.

More precisely: (a) photons with high energy will be reflected and focused only by the inner shells of the X–ray telescope. The reduced number of involved shells diminishes the source of "dispersion"; furthermore, the inner shells are probably less irregular. Both these effects improve the ability of focusing by the telescope with increasing energy. So the core radius is expected to be slightly smaller for high energy photons. (b) High energy photons have a wavelength nearer to the roughness size of the telescope shells than low energy photons, with an enhanced probability of scattering processes. This effect gives prominence to the wings of the PSF, which become, for higher energies, more important.

For the selected RUN we considered the following energy ranges: [140-170], [170-250], and [400-550] (in EDU).

By using an IDL procedure provided by Steve Sembay, we can determine the radial profile i.e., for each r the number of counts in the annulus between r and $r + dr$, divided the annulus area. Different binnings have been used for different radii. In the inner regions each bin is set to be equal to a pixel, for outer radii, bins are set to several pixels.

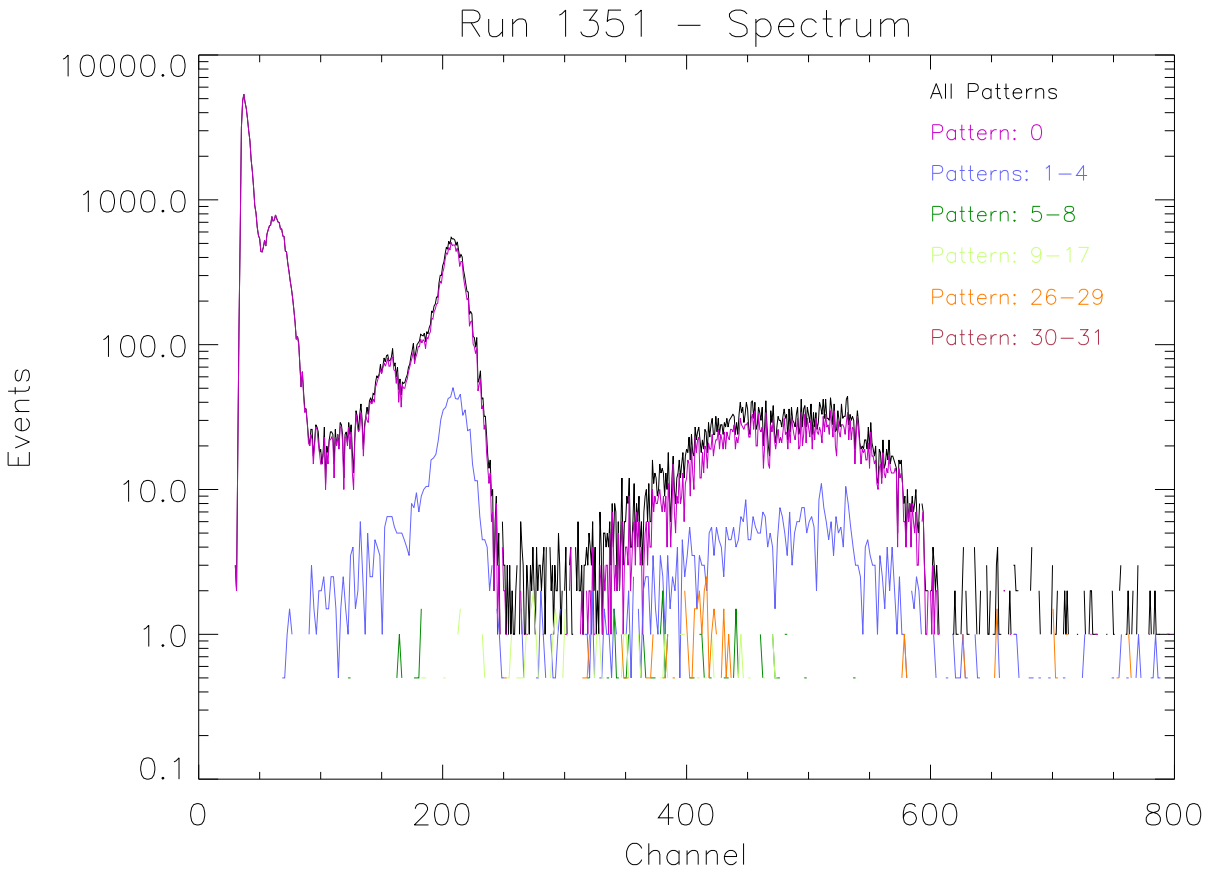

Figure 3: Energy spectrum with contributions from each class of pattern configuration: the main contributions is due to monopixels and bipixels confirming the absence of pile–up in the measurement.

In fact for large R where the number of counts is not very high, a large binning enhances the statistic making the integration procedure faster and it is anyway accurate. I divided the range (0-200) pixels in four regions with the following number of bins:

rmin: 0	rmax: 20	nbins: 20
rmin: 20	rmax: 40	nbins: 10
rmin: 40	rmax: 80	nbins: 10
rmin: 80	rmax: 200	nbins: 15

(*rmin* and *rmax* are in pixels units).

The IDL procedure evaluates the number of pixels in each annulus. It stores, for each pixel of the image, the bin which the center of the pixel belongs to. It assigns the entire pixel to the corresponding bin. For inner pixels, near the centroid of the PSF,

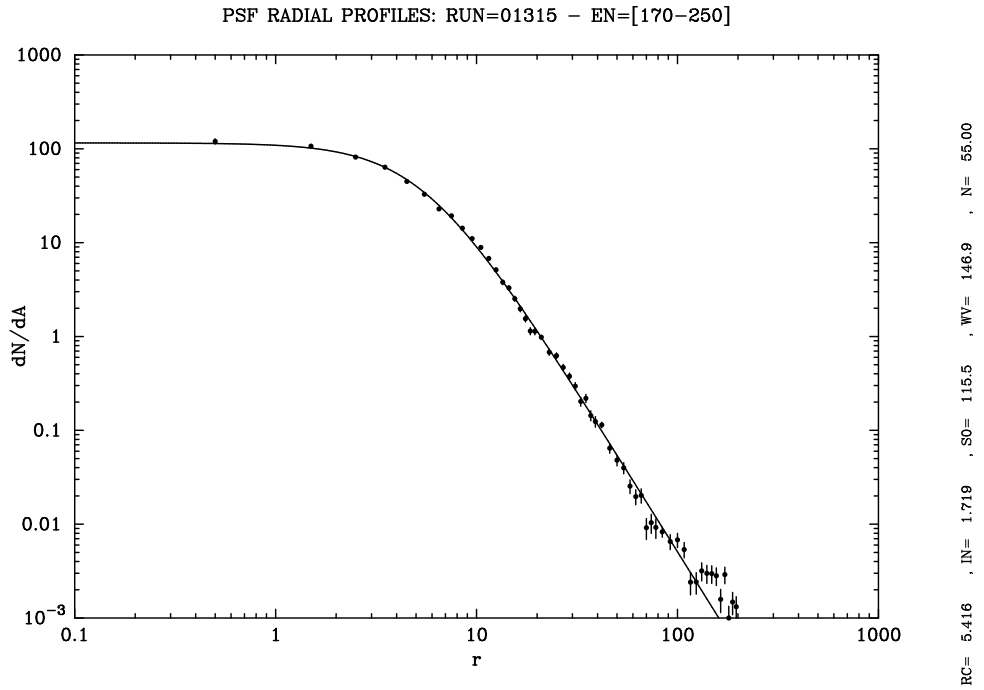

Figure 4: Radial profile for the PSF (RUN 01351) at 0.7 keV. The solid line is the best fit obtained using a King profile ((1)).

assigning a (squared) pixel to a (radial) bin, according to the position of the center, may be a rough approximation and this can introduce non negligible distortions. In fact, near the centroid where annuli curvatures are high, pixels can belong to different annuli in comparable fractions. Henceforth, I improved Steve's program adding a recipe suited to split pixels which are not completely included within an annulus. More precisely, the procedure runs over all pixels within a region R enclosing the RMIN – RMAX region and slightly larger than this. For each pixel, it finds the bin b_i which the pixel center belongs to and it checks if the circle enclosing the pixel (same center, $r = \sqrt{2}/2$) is fully enclosed in the same bin b_i. If so, then surely the same occurs for the whole pixel. In this case, the improved procedure "uses" Steve's program, and updates counts in b_i and the "area" of the bin summing the contribution of the pixel. Angular sectors are processed exactly as Steve does. Otherwise, if part of the circle is not in the same bin, maybe the pixel too is partly inside another bin. In this case, the pixel is split into *nsubpixels* subpixels (set by the user); each subpixel is processed by itself and provides a contribution to the counts equal to image(pixel)/nsubpixels and provides a contribution to the "area" equal to 1/nsubpixels (angular sectors are processed as in Steve procedure). I set nsubpixels=100, 49, 16, 4 for the four binning ranges.

In Fig. 4 we report the radial profile for the PSF for the RUN 01351 in the energy range [170-250] (corresponding to the 0.7 keV peak). For the other energy ranges, the

results are similar apart from the total normalization which depends on the total counts in the selected range of the spectrum. From the plot, it can be seen that a King function:

$$K(r) = \frac{A}{\left[1 + \left(\frac{r}{r_c}\right)^2\right]^{\alpha}} \tag{1}$$

represents a fair fit for the radial profile. The core radius r_c, the slope index α and the total normalization A are free parameters for fitting the data. In the figure, best fit parameters are reported, together to the χ^2 value and the number of data points used for the fit. The best fit parameters vary when other energy ranges are selected. In general, apart from normalization which depends on the total number of counts, the fit parameters have typical values of $r_c \sim 5.5$ (in pixels units; 1 pixel $\simeq 1.1''$) and $\alpha \sim 1.7$.

The main advantage in fitting the PSF profile with such a function consists of having a function which can be integrated analytically in rdr.

The Integral PSF (IPSF) provides for each radius r the total counts within r. To determine the cumulative profile we set $nsubpixels = 25$ over the whole radial range (0 - 230 pixels). Such cumulative profile is plotted in Fig. 5. The pink line shows the cumulative profile when the division in subpixels is not performed. It can be seen that even if the best fit profile is not heavily affected, the inner points show a certain discrepancy.

The present analysis must be extended to all the other measures. Before starting with systematic analysis, it is worth to fix some points:

- It is important to have a look at pattern distribution and at the spectra for events with a given pattern configuration because they provide a basic indication of the pile-up level;
- It is important to have a look at the spectrum of the central spot; maybe some peaks in the spectrum are due to "extra features" (e.g. bright pixels);
- An improved procedure for drawing radial profile for the PSF allows a better treatment of the inner part of the PSF;
- A King profile is a fair fit for the PSF, with two free parameters (apart from the normalization): the core radius and the slope. A King profile can be integrated in rdr analytically.

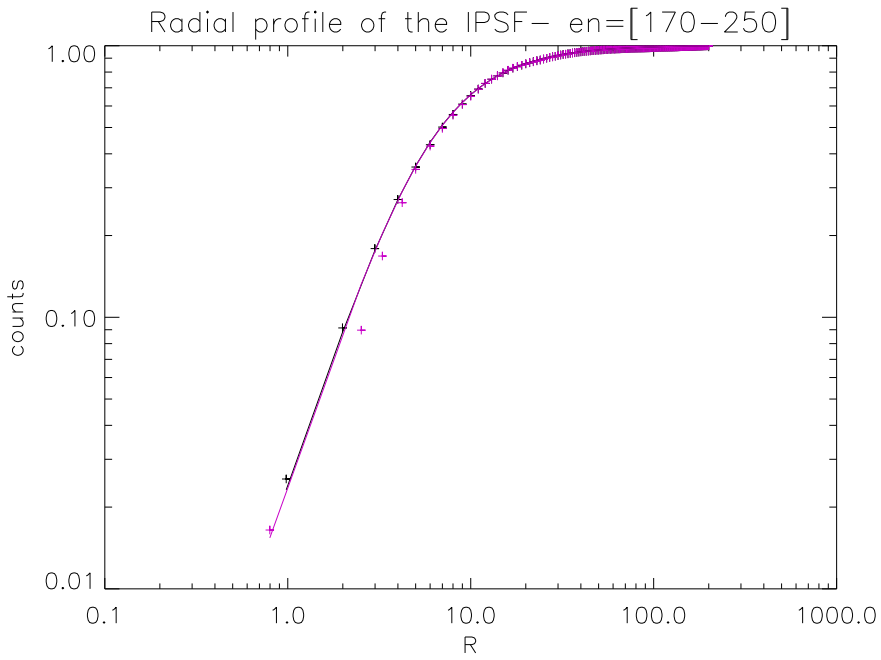

Figure 5: Cumulative radial profile for the PSF (RUN 01351) at 0.7 keV. The black data refer to the integral PSF when using *25 nsubpixels*. If no division in subpixels is applied (pink points) the inner points show a certain discrepancy.

3 ON-AXIS PSF

3.1 The algorithms for the systematic analysis

In order to carry out a systematic analysis for all the RUNS, I built a couple of procedures which automatically runs over all the available measurements. The first procedure includes two main parts:

- for each RUN, it performs a general recognition similar to the one described for the RUN 01351. All the RUNS are classified according to their pile–up levels. By means of pattern distribution and contribution of different classes of patterns to the spectrum, we divided RUNS in 4 pile-up classes. For each RUN, the algorithm determines the radial profile of the PSF. (see herebelow in this paragraph)

- In order to enhance the statistics, it stacks together RUNS with similar characteristics (same energy range, same pile-up level) and produced summed profiles (see §3.2 and §3.3).

The second procedure fits the radial profiles joining informations at different pile–up levels. The procedure and the results will be discussed in §3.4, §3.5 and §3.6.

Let's describe more in detail the part of the first procedure concerning the investigation of each single RUN. As previously mentioned, measurements for Al–K, Cu–K, Fe–L, Fe–K are available. For each line the following energy ranges are selected:

Al-K: $[300 - 550]$: main peak - en = 1.49 keV
$[1400 - 1700]$: bremsstrahlung

Cu-K: $[2200 - 2600]$: main peak - en = 8.1 keV

Fe-L: $[170 - 250]$: main peak - en = 0.7 keV
$[140 - 170]$: secondary peak
$[450 - 550]$: bremsstrahlung

Fe-K: $[1800 - 2000]$: K_α - en = 6.5 keV
$[2000 - 2150]$: K_β - en = 7.1 keV

Bremsstrahlung ranges have been taken avoiding contamination from pile-up energies secondary peaks. Monopixels and bipixels (patterns: [0-4]) are selected. The general inspection for each RUN (pattern distribution, spectrum for each pattern class, spectrum for the central spot) is performed in order to determine the pile–up level, and in order to investigate the presence of any peculiar feature. Just for the sake of example in Fig. 6, we plotted the spectrum of a measurements corresponding to the Al–K line. In addition to the K_α peak at 1.49 keV, some "multiple peaks" are present; the secondary peaks are located at multiple energies of the Al–K_α peak; this is an indication of a very high pile–up level. The higher peaks overlaps the bremsstrahlung contribution. Note that the selected bremsstrahlung energy range does not include any of the peaks.

It can also be seen that for high pile-up rates, patterns with an higher index become more important. In particular, this occurs for diagonal patterns (25-29) and patterns 30–31 which are directly related to piled–up events.

After the general recognition of each RUN, the procedure loops on the energy ranges for each selected RUN and for each energy range:

1. it finds recursively the centroid;

2. it processes the RUN for the current energy range only if events for those energies are not less than 300;

3. it builds 4 regions for radial profile
   + r=(0, 20), nbins = 20, nsubpixels = 100
   + r=(20, 40), nbins = 10, nsubpixels = 49
   + r=(40, 80), nbins = 10, nsubpixels = 16
   + r=(80, 230), nbins = 15, nsubpixels = 4;

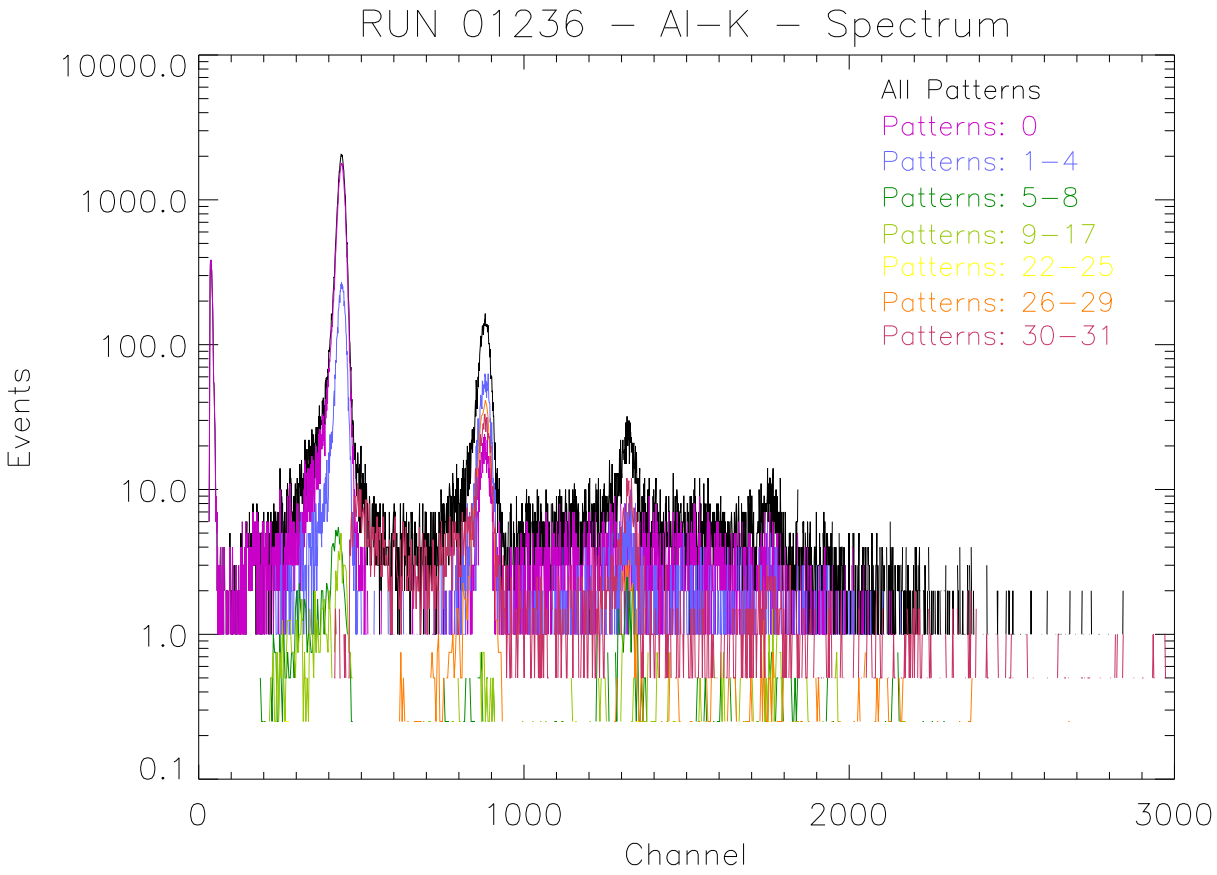

Figure 6: Spectrum for each pattern class for an Al–K measurements with a very high pile–up level.

4. if window mode occurs, it finds the maximum radius for radial profile and it considers only bins (with the same size as for Full Frame) within the maximum radius;

5. it determines the cumulative profile. For the integral PSF (IPSF) bins are set to 1 pixel for the whole range and *nsubpixels* is taken equal to 9.

3.2 Summing radial profiles

As mentioned in the previous section, in order to improve the statistic, it is worth to join different RUNS which are similar, i.e. which have the same degree of pile–up. The procedure is built in order to sum contributions coming from different RUNS. For each RUN, we must identify its pile-up level and (for each energy range) we can assign a group. We selected 32 groups (8 energy ranges times 4 pile-up levels). RUNS belonging to the same group can be joint. Actually we can not simply "sum" the two images and then

work out the sum profile, since in general different RUNS have not the same centroid. The presence of the mask on the CCD prevents us from translating images so as to match their centroids. On the contrary, we must determine the single profiles and then sum them together. The total profile p_t can be obtained summing n single profiles p_1,..., p_n, according to:

$$p_t = \frac{dN_t}{dA} = p_1 + ... + p_n = \frac{dN_1}{dA} + ... + \frac{dN_n}{dA} \tag{2}$$

where dN_i is the total counts number in the i–th bin (annulus) with inner and outer radii r and $r + dr$, while dA_i is the area of the annulus (not necessarily equal to $2\pi r dr$ because of the mask).

In the numerical algorithm we must account for the fact that dA is not the same for all the profiles and therefore for each bin b_i

$$p_t(b_i) = \sum_{k=1}^{n} \frac{N_k}{A_k}(b_i) \tag{3}$$

with errors:

$$\sigma_{p_t} = \frac{p_t}{\sqrt{\sum_{k=1}^{n} N_k}} = \frac{\sum_{k=1}^{n} \frac{N_k}{A_k}}{\sqrt{\sum_{k=1}^{n} \sigma_k A_k^2}} \tag{4}$$

When processing each RUN, two different situations can occur:

1. the current RUN is the first RUN processed of its group: in this case the procedure updates the total number of RUNS in the group (now equal to 1 because the processed RUN is the first) and it stores the RUN into a group list.

2. the current RUN belongs to a group which is not empty and (at least) another RUN of the group has already been processed. In this case the procedure reads the list of all the RUNS belonging to the group and

   - updates the list adding the current RUN;

   - determines and saves both PSF and IPSF profiles on the current RUN;

   - determines the PSF of the group and performs a fit;

   - determines the IPSF.

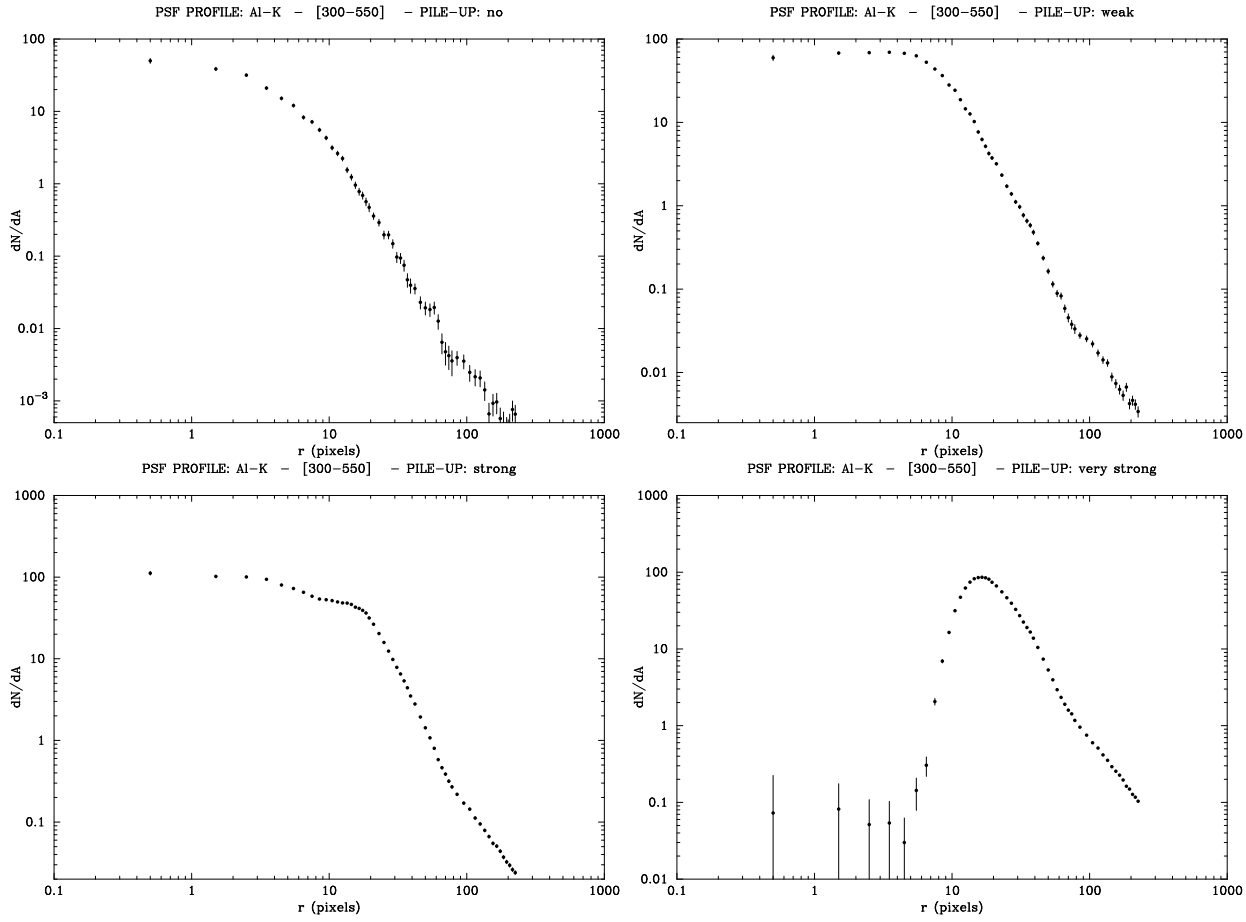

Figure 7: Spectrum for each pattern class for an Al–K measurements with a very high pile–up level.

3.3 Fitting

In Figs. 7 we plotted the profiles for the Al–K case for the four classes of pile–up level.

According to the general recognition carried out with RUN:01351, a King model is a fair fit for the radial profile, when pile–up is absent. However, as the pile–up level increases, in the inner part, the profile is damped and sometimes some irregular features appear. If the pile–up is strong at the center of the profile a "hole" appears. Accordingly, when fitting RUNS with pile–up, we must exclude from the data the inner points, in order to account for these distortions. Hence, depending on the different levels of pile–up we must select different radial ranges for fitting.

In order to check which ranges must be considered (or excluded) for fitting, we compared the different RUNS with different pile-up, for every energy range, plotting the ratio of each couple of RUNS.

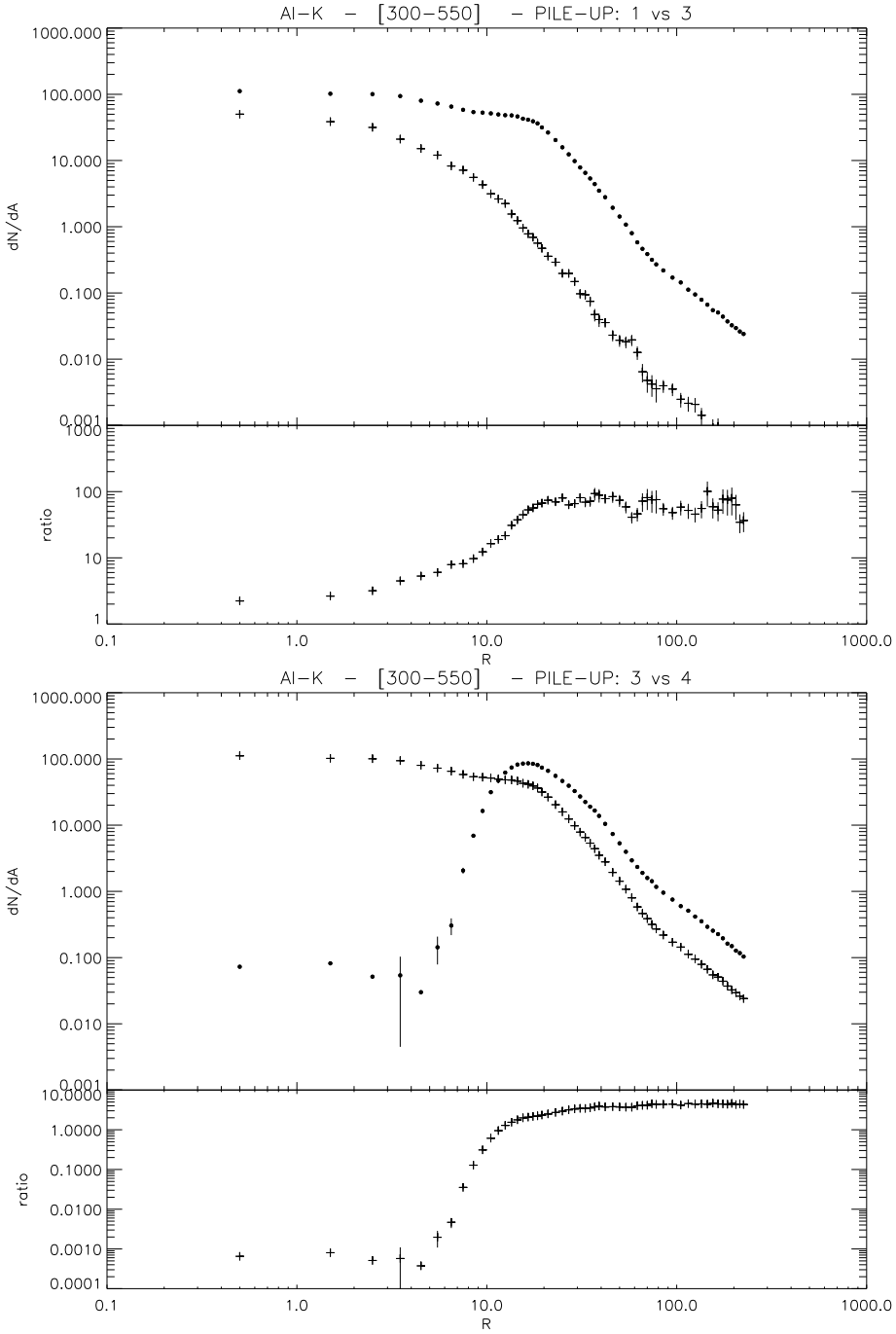

Figure 8: Ratios between profiles for Al–K at different pile–up levels (no pile–up vs. strong pile –up in the top panel; strong pile–up vs. very strong pile–up in the bottom panel)

As an example, in Figs. 8 we plot the ratio between two couples of profile for Al–K peak energy. In the top panel we compared the no pile–up profile and the strongly piled–up profile. The profile without pile-up has "good" data everywhere, on the whole radial range. However, counts on the wings are very few, so for no piled-up data we fixed $r < 200$. If we compare it with the weakly piled-up profile, the ratio is roughly constant at radii grater than 30 pixels. So we fixed 30-230 pixels as "good range". The "flat" range of the ratio determines the "good range" on which we can fit radial profiles. Analogously, in the bottom panel we compare the strong and the very strong pile-up. We can assume that the very strongly pile–up profile is reliable for $r \gtrsim 40$ pixels.

In general we imposed the following ranges:

no pile-up	0.1	-	200
weak	20	-	200
strong	30	-	230
very strong	40	-	230

This choice is suitable for almost all the situations. However, some problems have been found for some cases. Sometimes, a rough choice of the range can lead to a biased result and can significantly affect the value of the output best fit parameters. If the lower limit of the range is too small, the included points may start to suffer of pile-up effect and the profile in that region is a bit suppressed. The fitting profile starts to bend to outer radii, enhancing the output value of the core radius and makes the resulting fit unreliable. For these cases, we will adjust fitting ranges (see §3.5).

From Figs. 7, we can also see that for high pile up, where statistic is enough to model the wings, in the outer regions the profile shows a displacement from the King profile and it gets flatter. A correction must be inserted to the model profile in order to account for the behaviour of the wings.

Furthermore, it is worth to stack together informations in the various radial ranges (according to the different pile–up levels). So a stacking of all the RUNS of a selected energy range is needed. In the next paragraphs a detailed discussion about these points is provided.

3.4 Joint fitting of data sets with different pile–up levels

In order to make use of all the available informations, it is worth to consider contributions coming from different levels of pile–up, each of them within its good radial range. Another automatic procedure is used to fit simultaneously all the data sets, each within its selected radial range, using the same fitting profile with the additional requirement that the best fit parameters must be the same for all the data sets, apart from the total normalization.

3.5 Modeling the wings: King + Gauss function

As mentioned previously, the King model represents a fair fit for the radial profile, but where statistic is high enough to investigate accurately the wings behaviour, there a displacement from the King function is evident. In order to account for such a deviation, an additional contribution must be considered. Such a contribution must be negligible in the inner regions near the centroid where the King model provides by itself a sufficient accurate description, while it must dominate at larger radii. A King function plus a Gaussian contribution:

$$f(r) = N \left\{ \frac{1}{\left[1 + \left(\frac{r}{r_c}\right)^2\right]^{\alpha}} + \frac{R}{\sqrt{2\pi\sigma^2}} \exp\left[-\left(\frac{r}{\sigma}\right)^2\right] \right\} \tag{5}$$

suits well. This model function involves 4 free parameters (plus the total normalization): the core radius r_c and the slope α for the King component, the width σ for the Gaussian contribution, and the relative normalization R between the two components.

As usual, an initial guess of best fit parameters must be provided to fit the data . It can be verified that such initial guess must be accurate, otherwise some biased results can be reached. In order to fine–tune the initial parameters, I adopted a three step procedure.

- I fitted with a simple King model only the first set of data ('no pile–up'). In fact, in the inner part of the profile the "single" King function is a very precise fit. Correspondingly we get three best fit parameters: r_c, α, N.
- I froze the r_c and α inferred from the first step, and I performed a fit for the whole set of data using with the complete "King+Gauss" function (5), with $\sigma, R, N_1, N_2, N_3, N_4$ as free parameters. This hopefully provides some output parameters which are near to the best fit ones.
- Lastly, I thawed the r_c and α. The output parameters $\sigma, R, N_1, N_2, N_3, N_4$ of the previous step can be considered good initial guess for the fit of the whole data set with the function (5) where all the parameters are left free.

The automatic procedure stacks for each energy range all the data sets corresponding to the different pile–up levels, and fits simultaneously the curves with the (5) according to these three steps.

As mentioned in §3.3, the choice of the radial ranges for the different pile–up levels can be crucial; a rough estimation of the range can lead to biased results, since inclusion of damped region in the fit tends to enhance the output value of the core radius. When

the good fit range is not accurately selected, the parameters r_c and α (out of the first step and imposed as initial guess in the last step) change significantly. By increasing the lower limit of the cutoff of the radial range this effect fades, since inner regions are progressively excluded from the data set. At a certain cutoff we reach a stationary behaviour. The radius corresponding to the occurrence of the stationary behaviour is used as cutoff.

For the Cu runs (where weak indications of pile–up can be missed because they are out of the energy window) the RUNS we classified as "no piled–up" may have a very weak pile–up. Hence, we eliminated from the fit the first 3 points of the no–pile–up set.

The ranges have been updated as following:

	good ranges for fitting			
Al-K	no pile-up	0.1	-	200
	weak	20	-	200
	strong	40	-	230
	very strong	80	-	230
Cu-K	no pile-up	3	-	200
	weak	60	-	200
	strong	70	-	230
	very strong	80	-	230
Fe-L	no pile-up	0.1	-	200
	weak	30	-	200
	strong	35	-	230
	very strong	50	-	230

The RUN Fe-K has been rejected since it is a single RUN in window mode with a very strong pile–up. So the wings are not visible because of the window mode and the core can not be modeled because of the pile–up.

In the final analysis we concentrate on sum profiles for Full Frame, which are in general enough. For Al–K without pile–up we have no contribution in the [1400-1700] range in Full Frame, so we recovered the Partial Window mode.

In Figs. 9, we reported the cumulative set of data for each energy range with the best fit profiles. In Table 1 we reported the best fit parameters for each energy range.

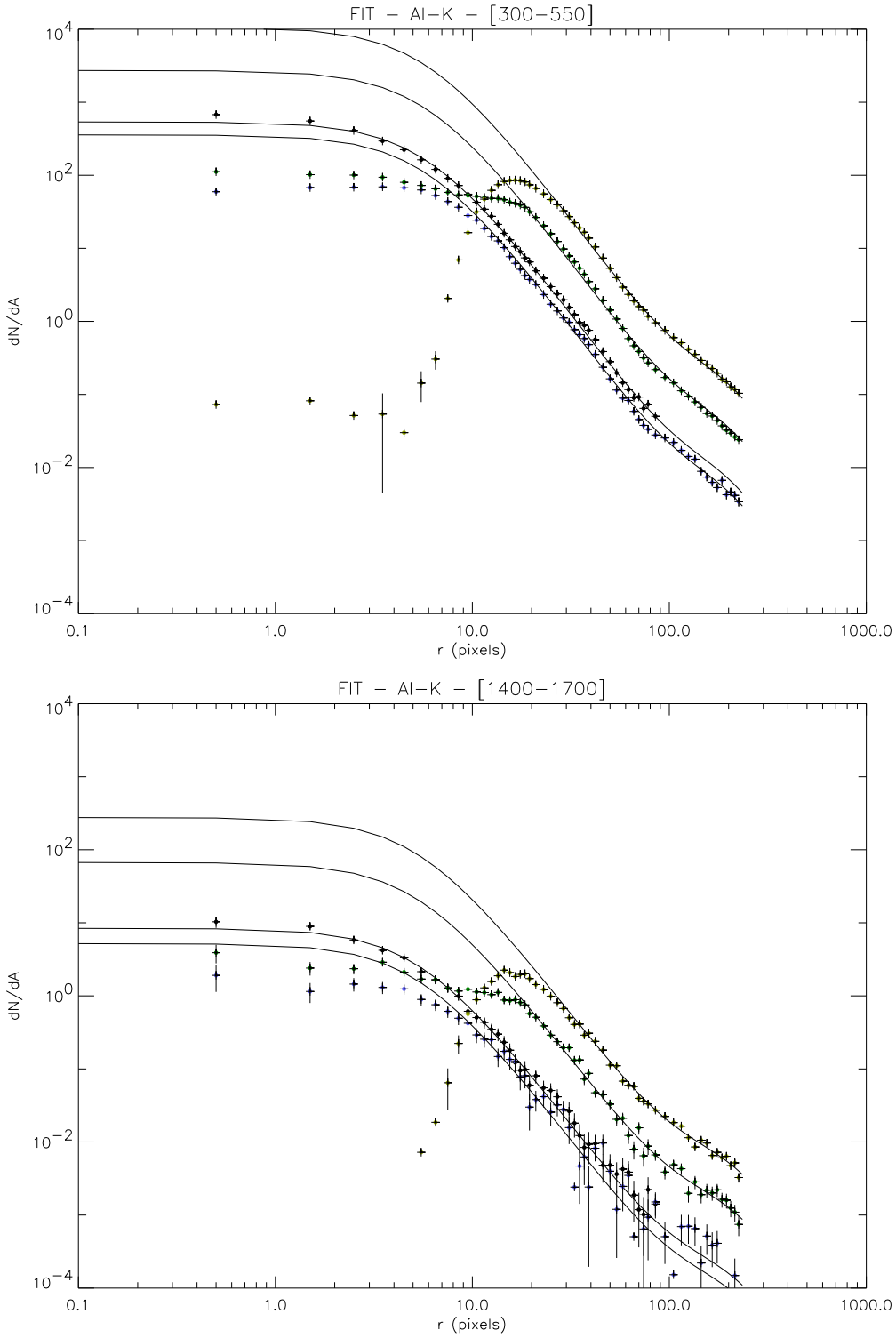

Figure 9: Best fit profiles:The four data sets refer to the radial profiles of the PSF at different pile-up levels. The best fit lines have all the same shape parameters but different total normalizations.(continues...)

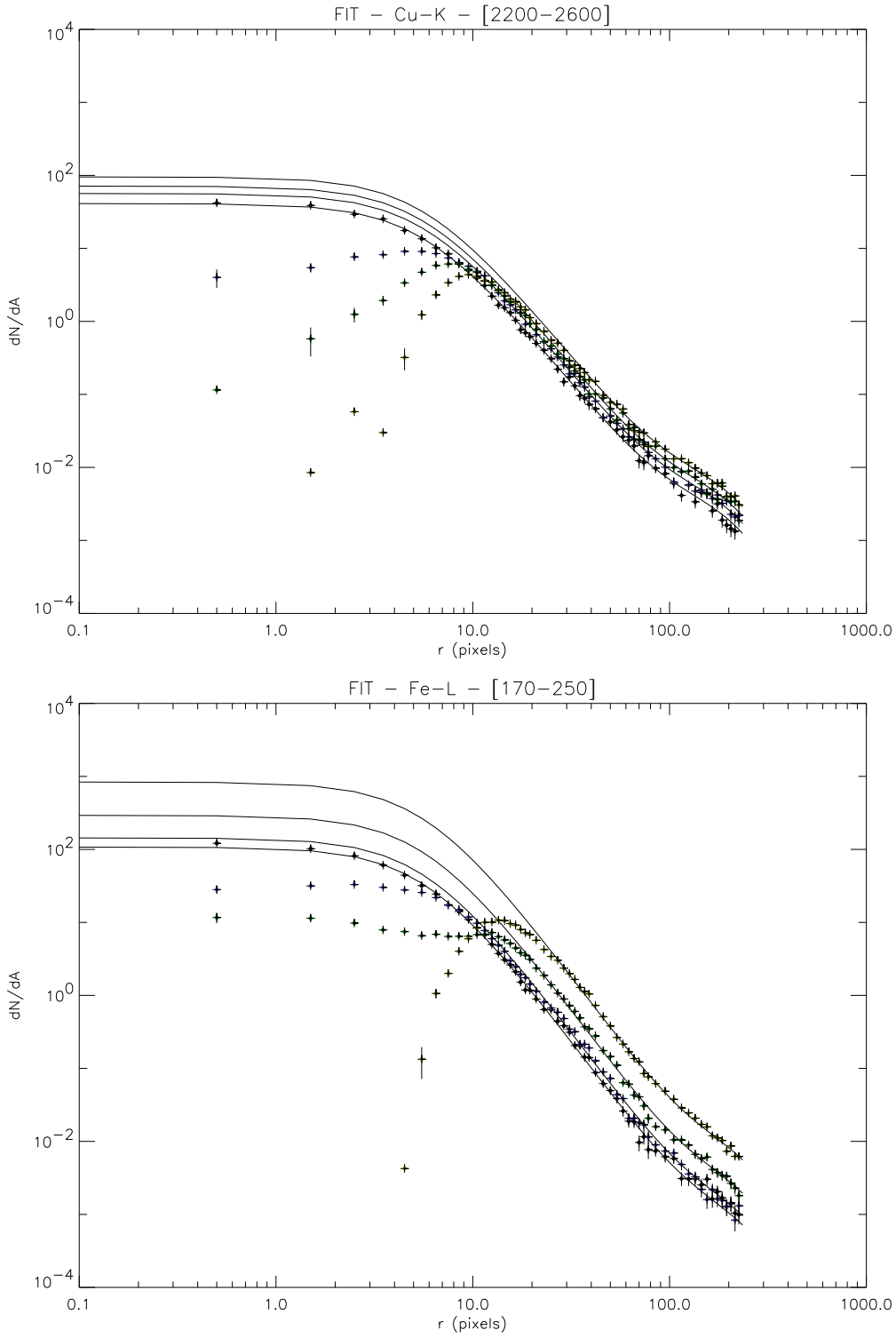

(...Fig. 9 continues): Best fit profiles.

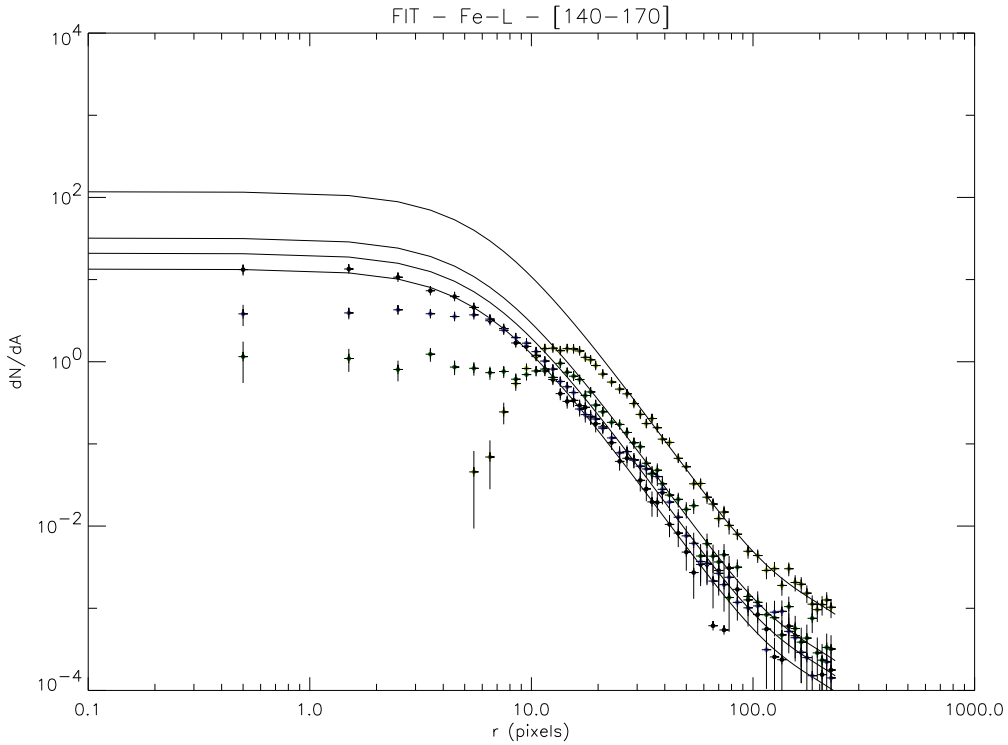

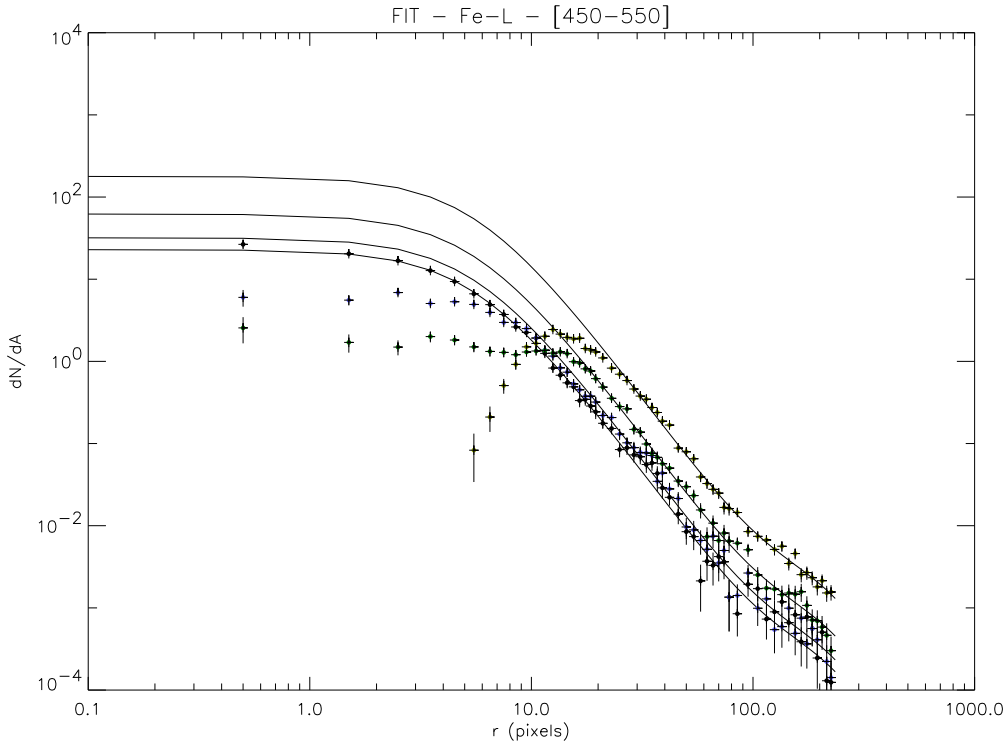

(...Fig. 9 continues): Best fit profiles.

Table 1: Best fit parameters

line	EDU	r_c	α	σ	R (10^{-2} units)
Al–K	300-500	5.923 ± 0.042	1.796 ± 0.007	137.18 ± 2.01	$2.427 \pm 0.052(^*)$
Al–K	1400-1700	5.388 ± 0.300	1.739 ± 0.048	150.79 ± 12.83	3.512 ± 0.447
Cu–K	2200-2600	5.707 ± 0.229	1.641 ± 0.027	137.10 ± 7.49	9.457 ± 1.070
Fe–L	170-250	5.860 ± 0.094	1.807 ± 0.015	156.51 ± 12.50	1.531 ± 0.100
Fe–L	140-170	6.223 ± 0.266	1.866 ± 0.044	198.31 ± 74.44	1.484 ± 0.217
Fe–L	400-550	5.700 ± 0.202	1.804 ± 0.034	146.56 ± 17.88	1.937 ± 0.254

Note : * This point has been reported in Fig. 10 with a 5 times greater error.

3.6 The radial profile of the PSF at different energies

Starting from Table 1, we can study the behaviour of best fit parameters at the different energies. The significant parameters (r_c, α, σ, R) are plotted in Figs. 10 versus energy (in keV).

The core radius of the King profile is almost constant. As expected it shows a weak trend to diminish for increasing energies. We fitted it with a straight line.

The slope α tends to diminish too, as the wings becomes more important at higher energies. We fitted the slope with a straight line.

The core of Gaussian component σ is constant (the first point has a very large uncertainty because of few points at large radii prevent us from safely modeling the wings region). This means that the point at which the contribution of the Gauss function starts, is the same at the different energies. We fitted it with a constant.

Lastly, the relative normalization R increases with the energy indicating that the contribution of wings increases with increasing energy, as expected. We fitted it with:

$$R(E) = (p_2 \cdot E + p_3) \cdot \exp\left[\frac{E^{p_4}}{p_1}\right] \tag{6}$$

with $p_4 = 2$ (frozen parameter).

Best fit parameters at the different energies are reported in each panel of Figs. 10. Summarizing, at large energies, the core is better defined, the power law is flattened, the radius at which the contribution of Gauss starts to be significant does not change, but its relative contribution with respect the King component becomes more important.

Globally, the PSF can be described by the following function:

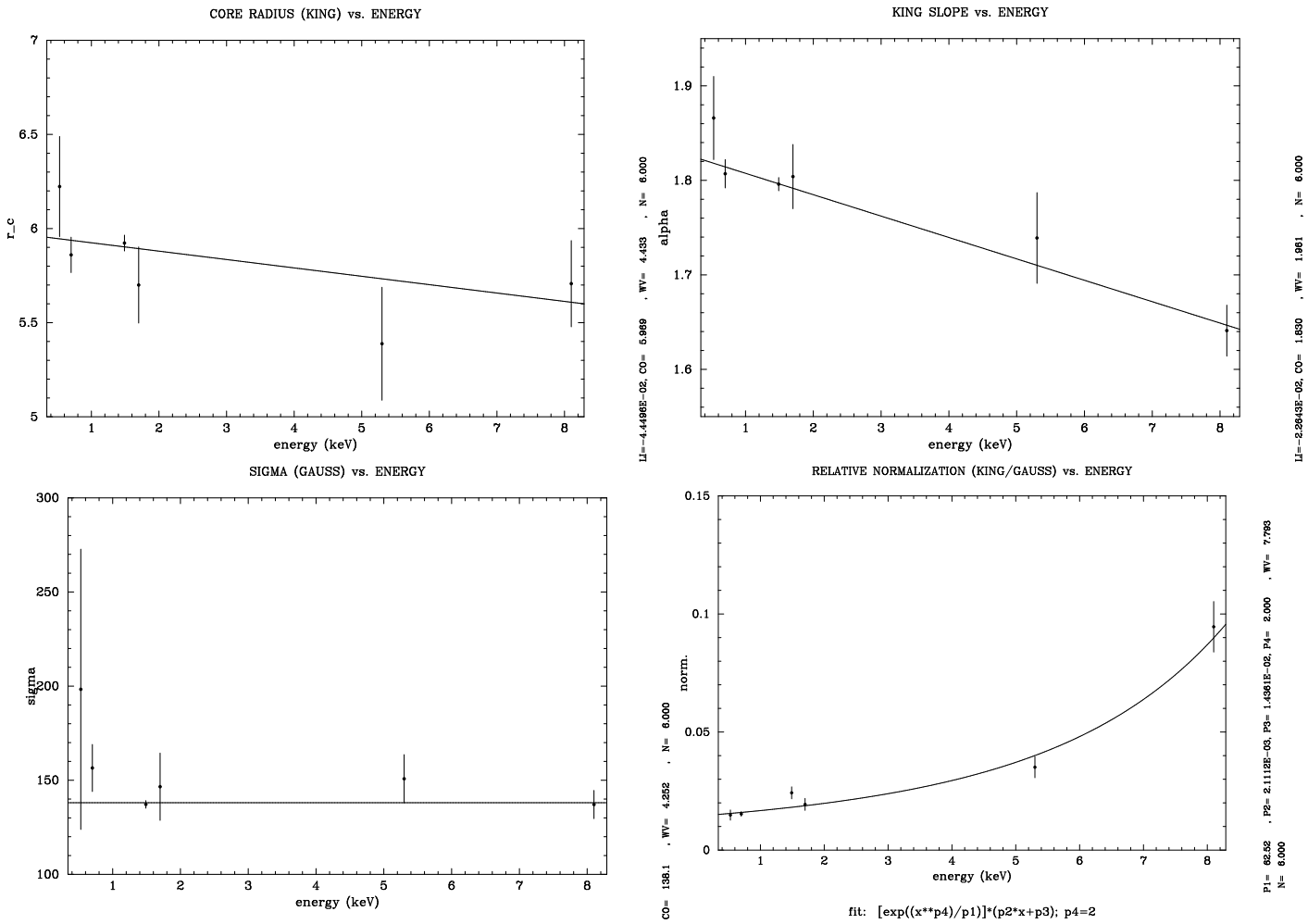

Figure 10: Best fit parameters at the different energies.

$$f(r) = \left[1 + \frac{R}{\sqrt{2\pi\sigma^2}}\right]^{-1} \left\{ \frac{1}{\left[1 + \left(\frac{r}{r_c}\right)^2\right]^{\alpha}} + \frac{R}{\sqrt{2\pi\sigma^2}} \exp\left[-\left(\frac{r}{\sigma}\right)^2\right] \right\} \tag{7}$$

with the parameters depending on the energy E (in keV) according to:

$r_c = a \cdot E + b$, $\quad a = -0.045 \pm 0.031$; $\quad b = 5.96 \pm 0.06$.

$\alpha = c \cdot E + d$, $\quad c = -0.023 \pm 0.004$; $\quad d = 1.83 \pm 0.01$.

$\sigma = 138.05 \pm 1.89$

$R = (em \cdot E + e0) \exp\left(\frac{E^2}{ew}\right)$, $\quad ew = 62.05 \pm 20.92$; $\quad em = (2.08 \pm 1.34) \cdot 10^{-3}$; $\quad e0 = (1.44 \pm 0.14) \cdot 10^{-2}$.

For the best fit of the relative normalization, different possibilities have been considered. Both $p_4 = 2$ and $p_4 = 4$ have been considered for best fit, and actually a strong difference is not observed, but anyway the fit $p_4 = 2$ seems to be closer to data. In the last panel of Fig. 10 the third point (at 1.49 keV) has been drawn with a magnified error (5 times greater) with respect to the one reported in Tab. 1. If the correct value is used in fitting, the very small error forces the fit to some distortions unless the em parameter is fixed (0.0025). The quality of the fit improves if this point is ruled out. If the greater error is assigned the fit is not very different to the one worked out when excluding the point.

4 OFF-AXIS PSF

The same procedures used for on-axis PSF analysis can be adopted for the calibration of the off-axis PSF for MOS–FM1. The off-axis PSF is different from the on-axis one and it presents distortions according to the azimuthal off-axis angle. In Figs. 11 we plotted some images of PSF at different angles and the distorted shape is evident. We neglect distortions and assume a radial profile. Even approximating to a radially symmetric profile, it is possible to measure variations of the PSF at progressively increasing off-axis angles.

The number of available data is not so large as for the on-axis PSF. Furthermore, on ground measurements are not really reliable because of the finite distance of the point-like

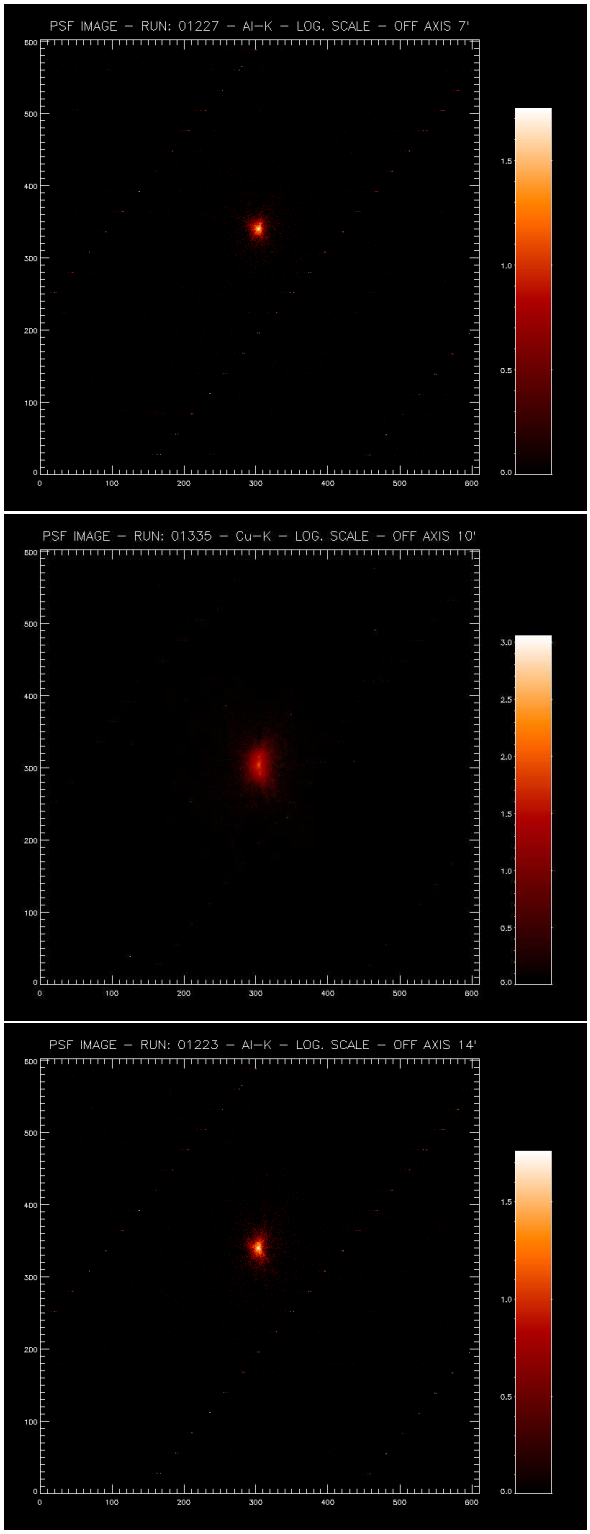

Figure 11: PSF images at different off-axis angles. The profile of the PSF is distorted

source. Apart from that, our purpose consists of building an automatic algorithm for the systematic analysis of the PSF. When on-flight data will be available the algorithm will allow a rapid analysis of the on/off-axis PSF.

We have a set of measurements for a 10' off-axis angle for 3 lines: Al–K, Cu–K, Fe–L, and for Full Frame (FF). So we can perform the same analysis we did for on-axis PSF. Unfortunately, unlike the on-axis PSF, most of measurements have a high – very high pile–up. So a modelization of the profile is often quite difficult and uncertain. Anyway (see forthcoming paragraphs) a general trend of parameters with off-axis angle can be drawn.

For 14' off-axis angle, we have only measurements for Al–K line and for the bremsstrahlung energy range only piled–up RUNS exist.

For 7' off-axis angle we have one only RUN for Al–K. As measurements concerning Al–K line are available at all the off axis angle, we can also (for 1.49 keV) analyze the behaviour of the fit parameters at different off-axis angles.

In order to produce radial profiles, perform the stacking between different piled–up levels and fitting the PSF profiles, we used the same procedures built for on-axis PSF.

4.1 10' OFF-AXIS ANGLE

As previously mentioned, only for this off-axis angle, measurements at different energies are available. Like the case of the on-axis PSF, the automatic procedure provides for each RUN the pattern distribution, the spectrum for each class of patterns, the spectrum for the central spot and the radial profiles, the cumulative PSF. The procedure also yields the sums of profiles in the same class (same energy range and same degree of pile–up).

For each energy range and for each pair of pile–up levels, the ratios of the profiles are determined in order to find the good ranges for fitting of each pile–up level.

Lastly, for each energy range, RUNS with different pile-up levels are stacked together and fitted simultaneously, with a King+Gauss profile, according to the same three step procedure described for the on-axis PSF. In Figs. 12 we plotted radial profiles for each energy range.

In Tab. 2 the values of the best fit parameters r_c (King core radius), α (King slope), σ (Gauss width), and R (relative normalization Gauss/King) are reported.

In Figs. 13, we can see how each parameter depends on energy. Actually measurements do not allow to provide clear conclusions; for Cu–K line (8.1 keV) for example we have only very piled–up measurements and the core fit is not very reliable. Anyway, a general trend can be drawn:

- core radius: the trend versus energy is similar to the on-axis case. As energy

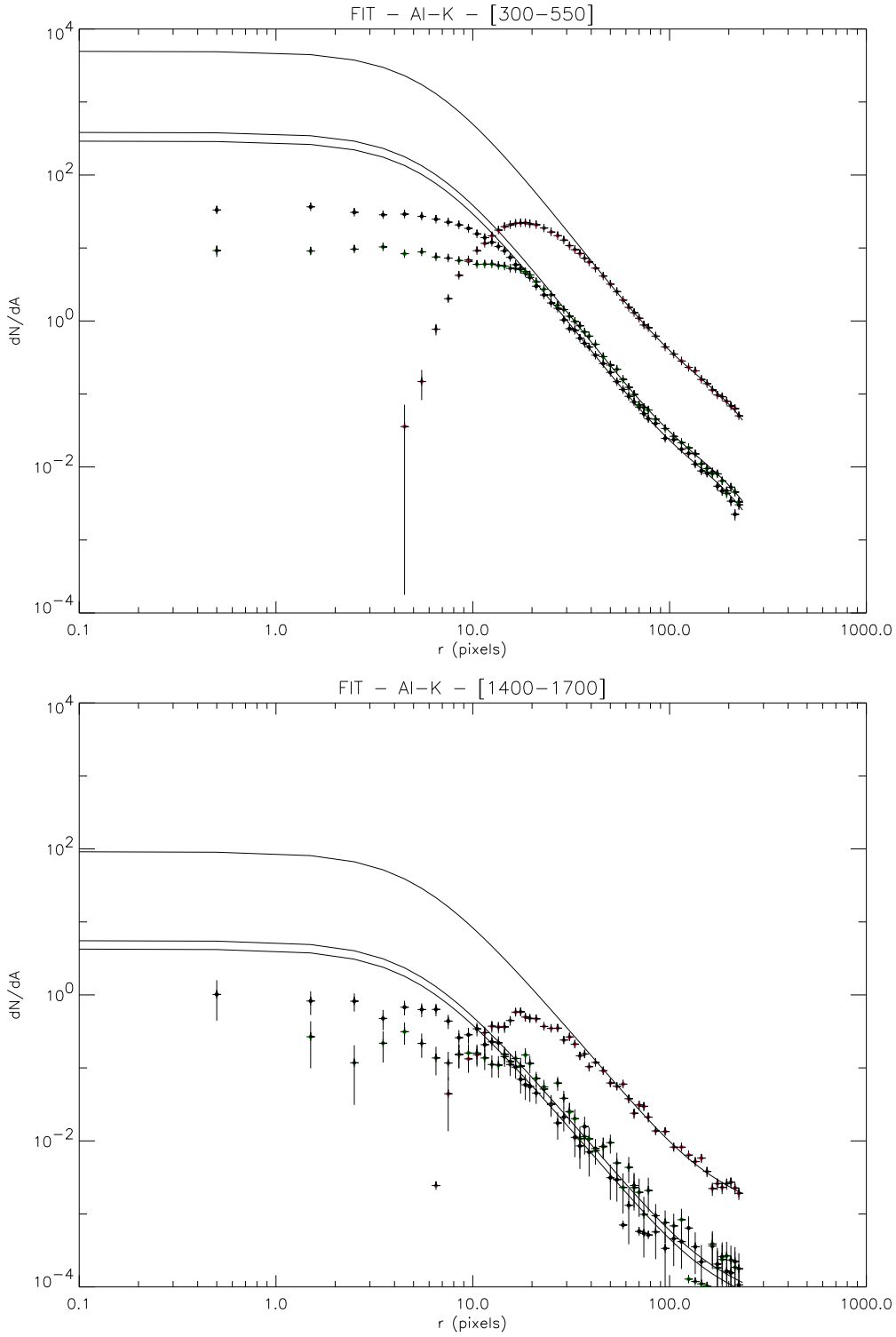

Figure 12: Best fit profiles for off-axis (10') PSF (continues...)

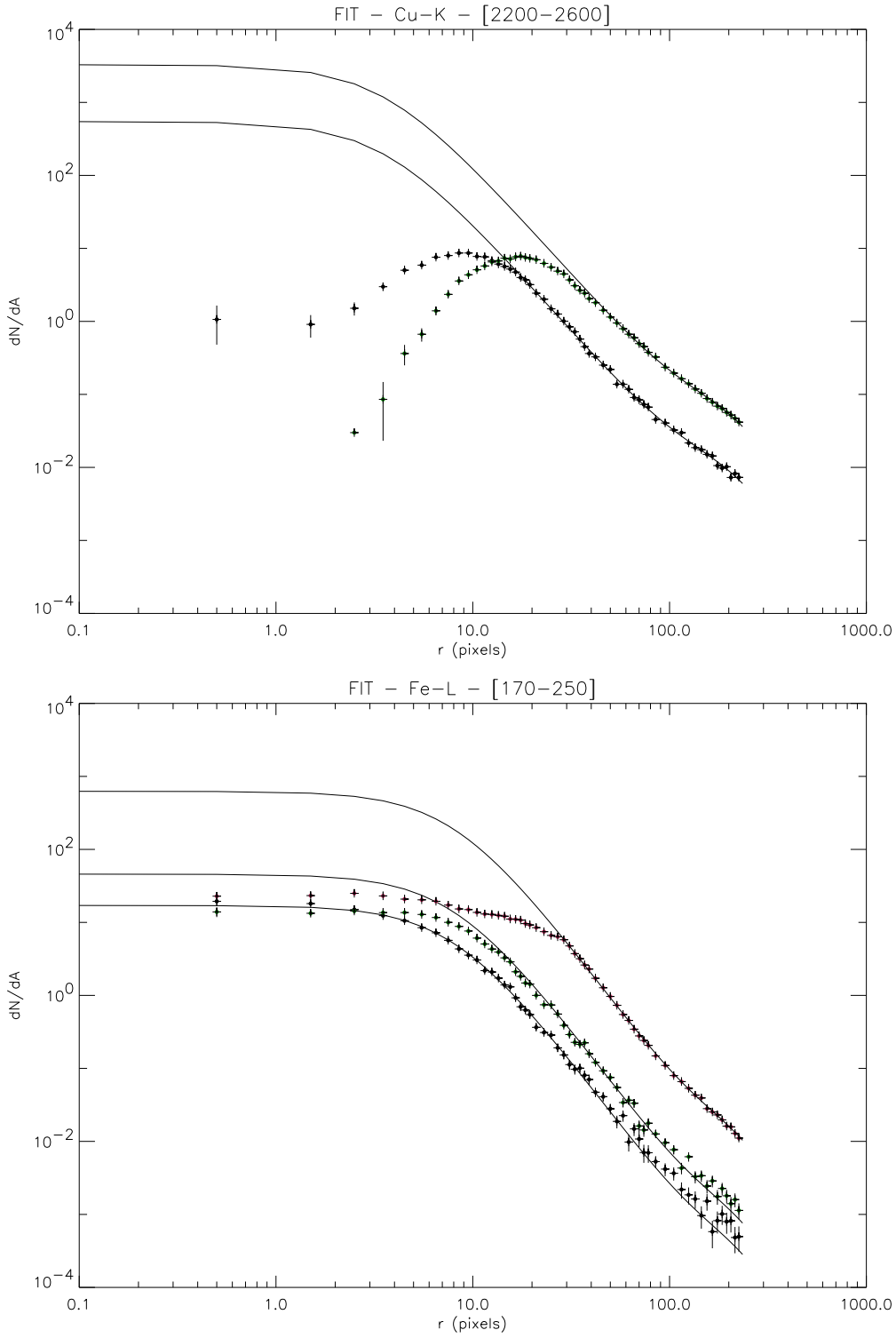

(...Fig. 12 continues): Best fit profiles for off-axis (10') PSF.

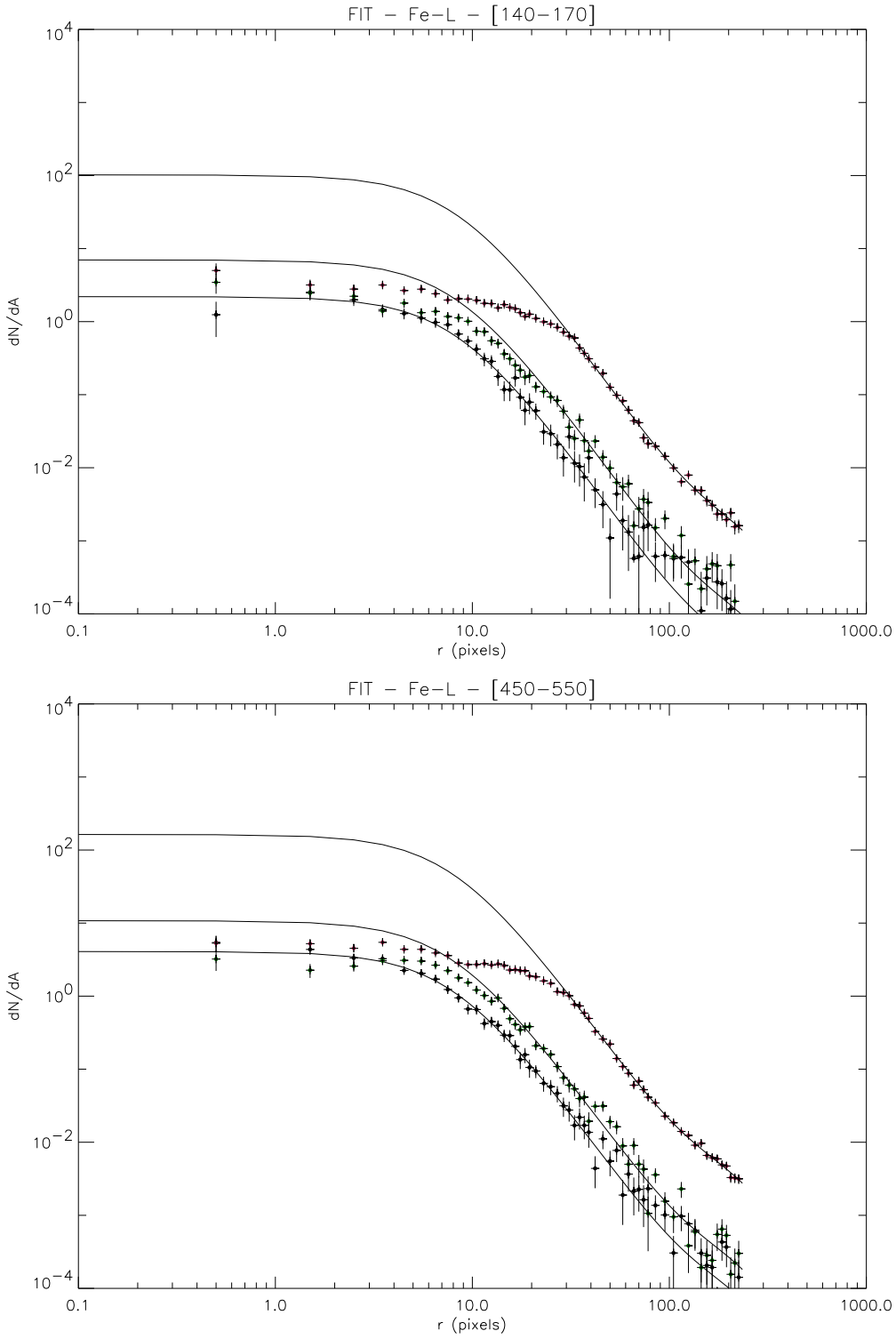

(...Fig. 12 continues): Best fit profiles for off-axis (10') PSF.

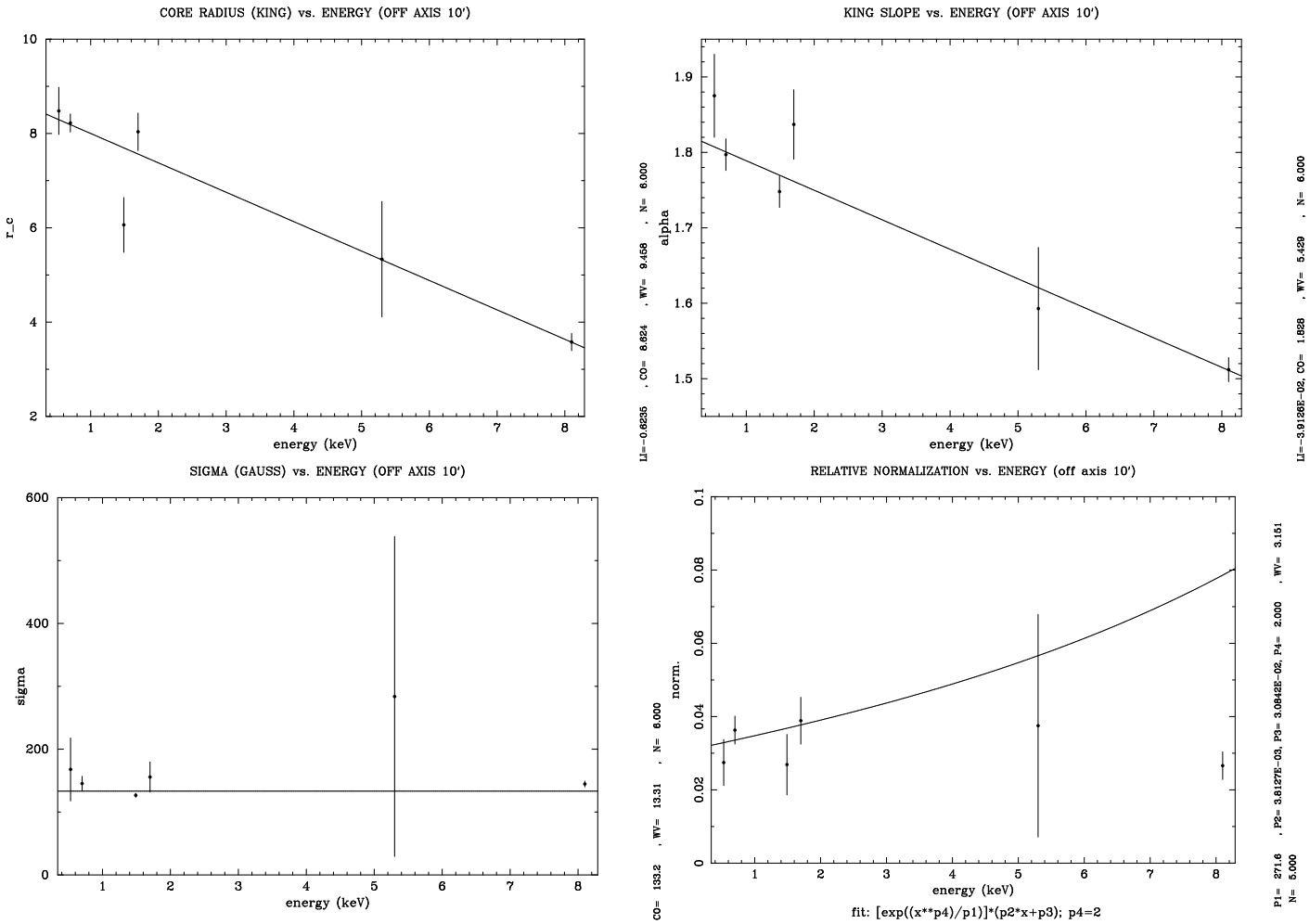

Figure 13: Best fit parameters at the different energies fir the off-axis (10') PSF.

Table 2: Best fit parameters for 10' off axis PSF

line	EDU	r_c	α	σ	R (10^{-2} units)
Al–K	300-500	6.062 ± 0.582	1.748 ± 0.021	126.74 ± 3.09	2.689 ± 0.825
Al–K	1400-1700	5.335 ± 1.223	1.593 ± 0.081	283.77 ± 254.40	3.751 ± 3.038
Cu–K	2200-2600	3.578 ± 0.183	1.512 ± 0.016	144.69 ± 4.65	2.661 ± 0.378
Fe–L	170-250	8.223 ± 0.192	1.797 ± 0.021	145.39 ± 11.48	3.632 ± 0.381
Fe–L	140-170	8.479 ± 0.501	1.875 ± 0.055	167.79 ± 50.13	2.746 ± 0.627
Fe–L	400-550	8.036 ± 0.397	1.837 ± 0.046	155.73 ± 23.99	3.888 ± 0.639

increases, the core radius diminishes. The slope of the linear best fit seems steeper than the on-axis one. At low energies the core is larger in this case than in the on-axis case. At high energies it seems that the enhancement due to the off-axis position is roughly balanced from the steeper fall towards small values.

- King slope: also in this case the trend with energy is the same than the on-axis case. The PSF has a flatter wing profile at higher energies (smaller α). Again, we can notice that the behaviour is steeper than the on-axis case; but unlike for core radius at low energies the slope is similar to the on-axis PSF. When energy increases the off-axis profile becomes flatter for the off-axis case. The off-axis angle and the increase of energy both contribute to flatten the profile.

- Gauss sigma: it is constant with energy and it is difficult to understand if values differ from the on-axis case even if it seems to be slightly smaller.

- Relative normalization: this is the only case in which we can notice a different behaviour with respect to the on-axis case. It can be well fitted with a constant (best value: $3.1533 \cdot 10^{-2}$). Anyway it is worth to stress that the last point (which constraint a flat behaviour) refers to the Cu–K measurements where the core is excluded by the very pile–up level; consequently, the King component can not reliably measured and correspondingly the relative normalization is also loosely constrained. If the Cu–K point is ruled out from the fit points, then the fit law used for the on-axis PSF is consistent with data (see the last panel in Fig. 13).

4.2 14' OFF-AXIS ANGLE

Here only measurements concerning Al–K are available. For bremsstrahlung energy range only very piled–up measurements have sufficient statistic to be analyzed. So only the peak energy (1.49 keV) can be reliably investigated. As usual RUNS are summed together, and in Fig. 14 is plotted the King+Gauss best fit regarding the 14' off-axis PSF, at 1.49 keV.

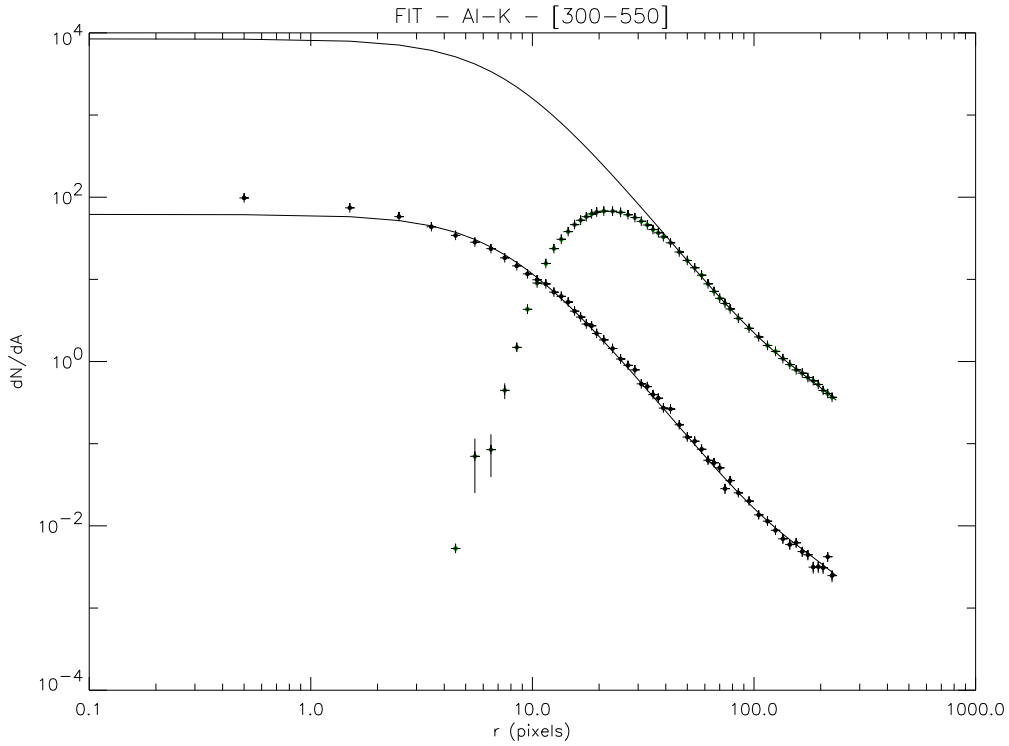

Figure 14: Best fit profiles for off-axis (14') PSF

The best fit parameter are the following:

line	EDU	r_c	α	σ	R (10^{-2} units)
Al–K	300-500	7.521 ± 0.095	1.639 ± 0.009	171.74 ± 4.18	7.573 ± 0.245

Of course in this case it is not possible to inspect the behaviour of parameters at different energies. The best fit parameters out of this data set can be used (see Sec. 5) to inspect the behaviour of PSF at different off-axis angles.

4.3 7' OFF-AXIS ANGLE

In this case only one RUN, at 1.49 keV (Al–K), is available. Probably there is a weak pile up, so we excluded some of the central points in fitting. In Fig. 15 the best fit profile (King + Gauss) for the 7' off-axis PSF is plotted.

Best fit parameters are:

line	EDU	r_c	α	σ (10^4 units)	R
Al–K	300-500	5.879 ± 0.187	1.610 ± 0.024	3.891 ± 96.434	0.342 ± 8.387

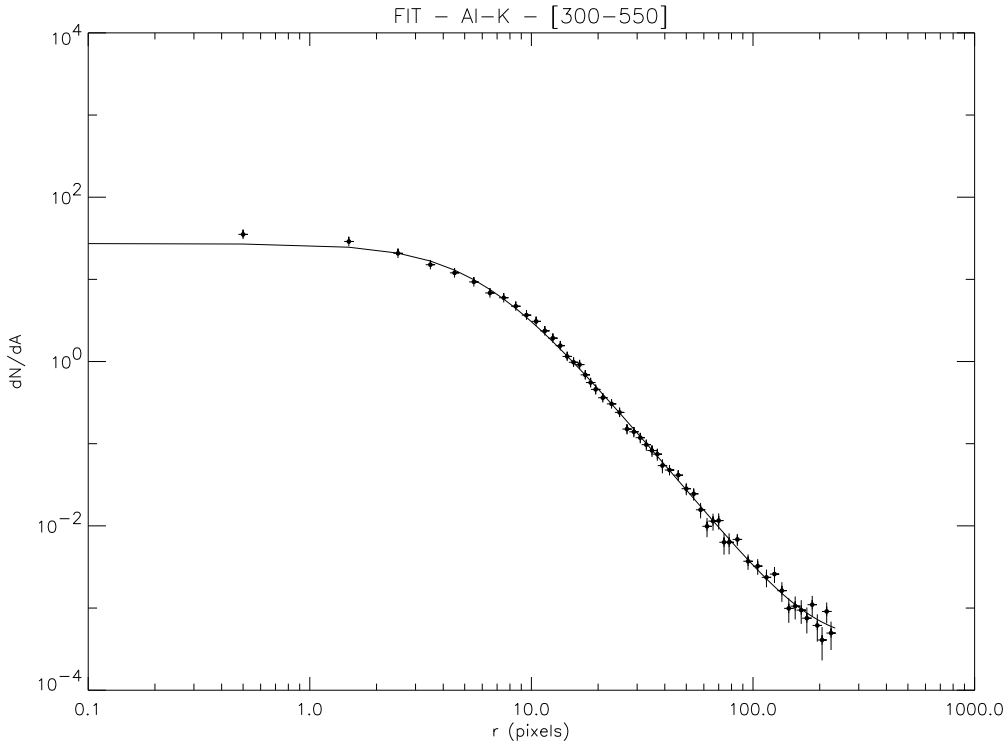

Figure 15: Best fit profiles for off-axis (7') PSF

Measures on the Gauss component are very uncertain, because of the poor statistic on wings.

5 Best fit parameters versus off axis angle at 1.49 keV

At 1.49 keV we have measurements at different off-axis angles: $0'$ (on-axis), $7', 10', 14'$. So wee can investigate the behaviour of best fit parameters when off-axis angle increases.

Figs. 16 report the behaviour of each parameter. The poor set of measurements does not allow to yield strong conclusions but, again, a general trend can be drawn. The core radius seems to be roughly constant in the inner part and increases at larger off-axis angles. The slope diminishes when off-axis angle increases, and the profile flattens The Gaussian sigma seems to be constant, and the relative normalization seems to increase at larger off-axis angles, where the importance of the wings increases.

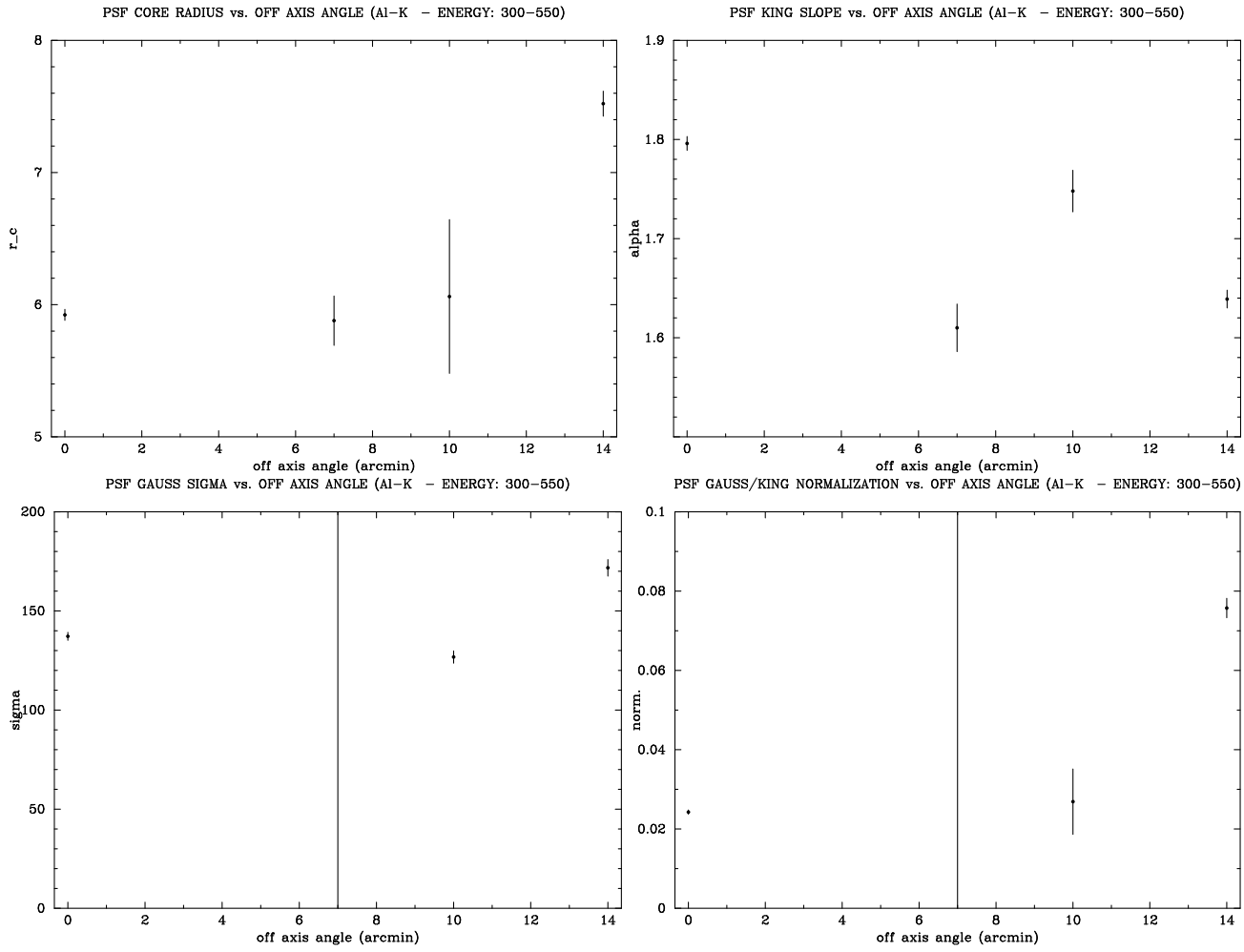

Figure 16: Best fit parameters at different off-axis angles, at 1.49 keV.

6 Summary

We have performed a detailed analysis of the on-axis and off-axis EPIC PSF using data from the Panter Campaign on MOS-FM1.

Our main findings can be summarized as follows:

- On axis and off axis PSF can be analytically modeled using a King + Gauss (eq. 7) function. The King component describes the core of the PSF while the Gauss component describes the wings
- For the on axis PSF a fair set of data allow to investigate the behaviour of best fit parameters with the energy. At higher energies the core of the PSF is better defined (smaller values) and the profiles gets flatter and the wings are more important.
- For the off axis PSF only a scarce set of data are available for the 10' off-axis angle. A general trend of parameters with energy can be drawn. The behaviour is similar to the on-axis case. The decrease of King parameters at increasing energies seems steeper for the off-axis PSF.
- For the 7' and 14' off axis angles, only measurements at 1.49 keV are available and the data set is poor. Anyway, a general trend of parameters with off axis angle (including the on-axis and 1' off-axis angle data) at 1.49 keV can be drawn. The PSF seems to get larger and flatter at larger off-axis angles.
- A satisfying description of PSF using the available data is possible only for the on-axis case and the off-axis case for the 10' angle. Only a general trend can be guessed for the other two off-axis angles and for the behaviour of parameters vs. off-axis angle at 1.49 keV. Nevertheless we have developed a fully automatic analysis system which we plan to use extensively on IN ORBIT CALIBRATION DATA to perform a complete calibration of the INFLIGHT PSF.